The potential of end-of-life ships as a floating seawall and the methodical use of gap resonance for wave attenuation

Wang, Gil; Bar, Daniel; Schreier, Sebastian

DOI
10.1016/j.oceaneng.2024.117246

Publication date
2024

Document Version
Final published version

Published in
Ocean Engineering

Citation (APA)
Wang, G., Bar, D., & Schreier, S. (2024). The potential of end-of-life ships as a floating seawall and the methodical use of gap resonance for wave attenuation. *Ocean Engineering*, *298*, Article 117246. https://doi.org/10.1016/j.oceaneng.2024.117246

Ocean Engineering 298 (2024) 117246

Contents lists available at ScienceDirect

Ocean Engineering

journal homepage: www.elsevier.com/locate/oceaneng

The potential of end-of-life ships as a floating seawall and the methodical use of gap resonance for wave attenuation

Gil Wang [a,b,*], Daniel Bar [b], Sebastian Schreier [a]

[a] Delft University of Technology, Mechanical, Maritime and Materials Engineering (3mE), Department of Maritime and Transport Technology (M&TT), Sec. Ship Hydromechanics, Delft, 2628 CD, The Netherlands

[b] Coastal and Marine Engineering Research Institute (CAMERI), Technion Israel Institute of Technology, Haifa, 3200, Israel

ARTICLE INFO

Keywords:
Ocean and sea space utilization
Floating structures
Floating breakwaters
Hydrodynamic interaction
Wave transmission coefficient
Gap resonance

ABSTRACT

This study examines the potential of a new type of floating seawall, made up of retired large-scale oceangoing vessels, to be used in open water and exposed coastal areas. The main objectives of the research are to assess the effectiveness of the floating seawall concept, to determine the contribution of the gap resonance to wave attenuation, and to compare the results of physical tests with those obtained numerically using ANSYS-AQWA. The use of end-of-life ships in this way provides a unique opportunity to extend their life cycle and reduce the environmental and human health risks associated with the current practice of shipbreaking. The research focuses on a multimodule floating seawall configuration, where each module is composed of two hulls that are rigidly connected side by side, with a small gap to induce gap resonance. The results suggest that end-of-life ships can be used as a resource for the construction of floating seawalls for various marine applications. Furthermore, the results demonstrate the positive influence of the gap resonance on the wave attenuation capacity of the seawall, as well as the limitations of the numerical tool in providing realistic values in this region.

1. Introduction

1.1. Context

With the recent IPCC sixth assessment report and its message of climate change disillusionment, coastal urbanization, and increasing population growth, the advantages of sustainable development offshore are clear and more widely accepted (Glavovic et al., 2022). This research investigates the performance of a novel floating seawall system in deepwater conditions during typical storms in the North Sea and the Eastern Mediterranean Sea. The main objectives of the current research are to evaluate the effectiveness of a novel floating seawall concept, constructed entirely from end-of-life ships, to evaluate the contribution of gap resonance to the wave attenuation, and to examine the agreement between the physical testing and the results obtained numerically.

Floating structures can provide a sustainable platform for a wide range of offshore activities, including renewable energy, storage facilities, coastal protection, commercial and recreational spaces, and even residential purposes (Lamas-Pardo et al., 2015; Wang et al., 2019). However, the main limitation of most ocean and sea space utilization projects is that they work best in an environment free of waves, which limits the performance of the structures in both operational and structural aspects to a certain sea state (Wang et al., 2020a). In sheltered water, floating structures can sometimes be the preferred building alternative. It could be cheaper, more sustainable, and better predicted than building in the soil. Floating structures are not prone to soil subsidence, earthquakes, or the negative effect of increased groundwater (Anon, 2007). But, more importantly, the additional space created by floating platforms does not substitute for green fields (nature reserves) and can manage the sea level rise effortlessly (Wang et al., 2020b). The conceptual floating breakwater investigated in this research forms a protective seawall, positioned perpendicular to the main propagating wave direction. To shield any type of sea space utilization project located at its leeward side and therefore to increase their performance limits in heavier sea states.

1.2. Motivations

The primary motivation for the current research is to increase the prospects of ocean and sea space utilization projects in open water

* Corresponding author at: Delft University of Technology, Mechanical, Maritime and Materials Engineering (3mE), Department of Maritime and Transport Technology (M&TT), Sec. Ship Hydromechanics, Delft, 2628 CD, The Netherlands.
E-mail address: wang@technion.ac.il (G. Wang).

https://doi.org/10.1016/j.oceaneng.2024.117246
Received 19 October 2023; Received in revised form 15 February 2024; Accepted 20 February 2024
Available online 28 February 2024

conditions, by decreasing the impact of sea and ocean waves using a floating seawall. Searching for a sustainable way to approach the task, this research suggests the use of end-of-life ships as the main building resource for the construction of the floating seawall. The life expectancy of an ocean-going cargo vessel is only around 25 years (Solakivi et al., 2021), and in most cases, the integrity of the structure, when it reaches its end of life, is still adequate.

The Circular Economy approach not only helps reuse currently available resources, but also helps mitigate the chance of non-regulated shipbreaking, the norm of ship disposal to date (Jain et al., 2017). Although most of the ships are owned and controlled by high-income economies (e.g., the EU, the United States, South Korea and Japan), between 2014 and 2018 around 80% of the end-of-life ships were demolished in Bangladesh, India, and Pakistan. Where recycling yards in these three countries are known for their infamous 'beaching method' that strands ships on the coast and dismantles them using unskilled labor (Wan et al., 2021). This is without regard to current shipbreaking conventions and regulations such as the Basel Convention, the Hong Kong Convention, and EU regulations.

1.3. Description and approach

The current research is a physical and numerical study that examines the wave structure interactions of a floating seawall in 2D. It aims to determine the capacity of the chosen model arrangement to attenuate the incoming beam waves. Physical testing is carried out in a two-dimensional testing environment in the towing tank facility at the Ship Hydromechanics Laboratory in TU Delft, together with the numerical model that has been programmed in the ANSYS-AQWA.

The modules composing the floating seawall are aimed to represent the cargo hull space of an end-of-life oceangoing vessel of approximately 360 m in length. Where the cargo hull is 80% of the total length and generally rectangular in shape. The environmental conditions in this research include storms with wave periods of 10 to 15 s, which are typical for annual and extreme events in both the North Sea and the Eastern Mediterranean Sea (Levin et al., 2019; Lavidas and Polinder, 2019).

A 400,000 DWT ORE Bulk Carrier class is considered a reference vessel in this investigation. Currently, there are more than 30 vessels of this type in active service, where the first ones were built in 2011 and 2012 (Yang, 2016) — meaning that in the next decade or two they will reach their end-of-life, and most likely will be sold for scrapping. The reason for choosing these vessels over any other cargo ships is arbitrary, but their main particulars, do make them great candidates for floating seawalls; mainly due to their large beam (B) of 65 m (Drimer et al., 1992).

To improve the attenuation capacity of the seawall, each rectangular module (which acts as a simplified representation of the hull) is rigidly connected alongside an equal module. Forming a twin-hull configuration with a gap (clearance between the two hulls) of B/2. This gap is a methodical design choice for generating intermodule gap resonance at a wave period of 12 s. The two hulls are connected with a rigid cross-structure connection that can be calculated under the current classification regulation, where the typical section modulus of the cross-structure benefits enormously from the depth of the hull (D) given in Table 1. A good reference for this structural approach can be found in Allseas's Pioneering Spirit, which was designed and built to install and remove offshore platforms and has almost similar overall dimensions with twice the clearance size between the hulls. However, as the proposed seawall structure is intended to operate in gap resonance regions, and not avoid it, attention should be paid to the fluid motion in the gap which is severe and may produce a potential crisis for the safety of the cross-structure.

As this research only considers beam waves, the model is located perpendicular to the walls of the towing tank in all the configurations tested. Therefore, to have a floating seawall system consisting of at least three modules, the module length could not exceed 1.2 m. Therefore, the chosen scale factor for this experiment is 1:250, motivated mainly by the distance between the walls of the towing tank (4.22 m). Fig. 1 shows the schematic arrangement of one module in relation to the reference vessel, and Table 1 provides the related main particulars.

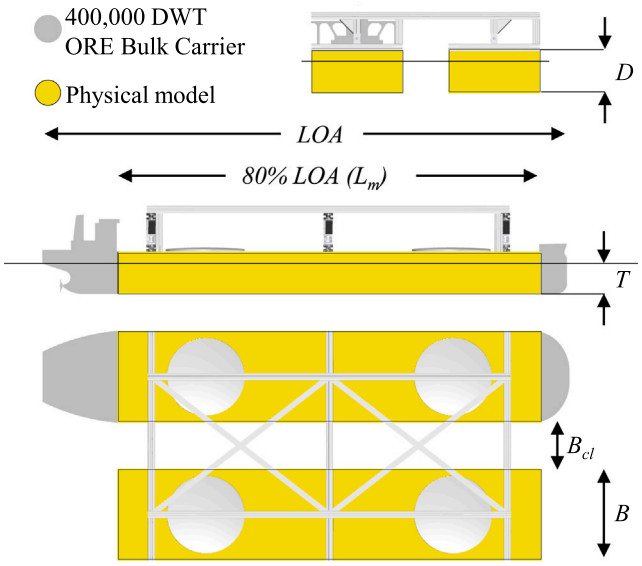

Fig. 1. The typical box-shaped module used in the current investigation overlaid in the shadow of a 360 m, 400,000 DWT ORE bulk carrier.

Table 1
Main particulars of the reference vessel and physical model.

Description	Ω	Units	400k DWT	Model
Length over all	LOA	(m)	365.0	–
80% LOA	L_m	(m)	300.0	1.200
Beam	B	(m)	65.0	0.260
Depth	D	(m)	30.0	0.120
Draft	T	(m)	23.0	0.092
Displacement	Δ	(ton)	450k	0.029
Clearance (hulls)	B_{cl}	(m)	32.5	0.130

In the current research, the physical testing procedure measures the response amplitudes of floating modules and wave elevations before and after they interact with the moored model. Numerical analysis in the time domain is programmed to simulate the exact same conditions as in the physical environment. The acquired data from the physical tests are used to evaluate the numerical results before additional configurations are developed. Compared to the physical testing process, the numerical platform provides a much easier path to explore additional model configurations and design alternatives.

1.4. Literature review

Floating breakwaters have been academically and practically investigated throughout the last century. This includes also their actual implementation during World War II (Carr, 1951; Hartcup, 2006). Thus, 'standing on the shoulders of giants', this research includes some of the advancements and improvements made throughout the years, which may be relevant in the context of retrofitting end-of-life ships - typically 300 m in total length, or larger. A review of relatively recent research and developments on floating breakwaters reveals that this topic has been dominated by approximately a half dozen breakwater designs (Dai et al., 2018). Current research has focused on rectangular box-type structures to represent the crude geometry of ocean-going cargo ships, where approximately 80% of the total length of the ship is box-shaped. Therefore, attention was paid to research related to these

specific configurations, such as: 'the box type' (Drimer et al., 1992) or 'Pontoon type' (Sannasiraj et al., 1998). For example, two-legged breakwaters have been shown to increase the efficiency of conventional box-type floating breakwaters (with equivalent shape and mass) by up to 35% (Masoudi and Gan, 2021). Gesraha (2006) reports that the attachment of two side plates results in higher added mass and heave damping coefficients, where the other damping coefficients are lower. Furthermore, in his study, the transmission coefficient (C_t), given in Eq. (1) below, at beam waves is reported to be lower compared to a regular rectangular floating breakwater.

$$C_t = H_t / H_i \tag{1}$$

Here, H_t is the transmission wave height and H_i is the incident wave height.

The contribution of a longitudinal center plate on a box-type floating breakwater has also been investigated and reported in several published studies, e.g. Koraim and Rageh (2014), Yang et al. (2018). However, these two studies do not mention the contribution of using a twin-hull configuration. Peña et al. (2011), reports that the contribution of a twin-hull configuration (with relatively small clearance) increases wave dissipation and improves the performance (lower transmission coefficient) of the floating breakwater relative to a single hull. This point is also widely accepted, since beam (B) is considered a fundamental parameter when designing a floating breakwater (Drimer et al., 1992). However, there is no explicit explanation for the contribution of the gap between the two hulls in relation to the gap resonance at a specific wavelength.

In the practice of ship-to-ship mooring, gap resonance is considered an extreme loading condition that can induce severe loads on the mooring system (lines and fenders) and hinder the intended operation and handling (Zhao et al., 2018). In recent years, the influence of gap resonance has been increasingly investigated, as ship-to-ship (or side-by-side) offloading became a commonly used practice in the offshore industry for FLNGs and FPSOs (Zhou et al., 2023; Gong et al., 2023; Gao et al., 2020, 2022). However, the focus of these studies is mostly on multi-body hydrodynamic interaction and the limitation of potential flow solvers to provide adequate results (He et al., 2022; Zhao et al., 2017; Huijsmans et al., 2001). In addition to studies on free surface effects, within the narrow gap, playing significant role in the field of wave energy converters (WEC) (Gao et al., 2021, 2019). To our knowledge, there are no explicit studies on the performance enhancement of floating twin-hull breakwater configurations by gap resonance, nor research on the use of end-of-life oceangoing vessels to construct such configurations.

1.5. Model configurations

The current research investigates one model spatial configuration: "Scattered" and three types of sectional configuration: "Upright hydrostatic", "Two legs", and "Inclined". Most of the configurations are tested numerically, and only the "Scattered" + "Upright hydrostatic" configuration is tested using a physical model. The configurations of the sectional model are shown in Fig. 2.

The Scattered configuration considers three all-equal modules and their associated mooring system. In this configuration, the modules are not connected to each other, and they are spread out (in plan view) to allow free-floating movement of the first order, while kept in place using a compliant mooring system. This layout is selected for both safety and operational considerations, mainly to allow sufficient margins to prevent collision when moored in open water conditions.

To further examine the performance of the twin-hull module, we evaluated optional modifications to the existing hulls using additional sectional configurations. However, to minimize the ecological impact when converting end-of-life ships into floating seawall modules, the extent of possible modifications is minimized, and two types of modifications are examined: "internal" and "external". The internal modification is directly related to the weight and its location, which can be used to determine the draft and floating condition (pitch and heel angles) of the module. The external modification examines the influence of an external two-legged structure, which has shown great promise in related research.

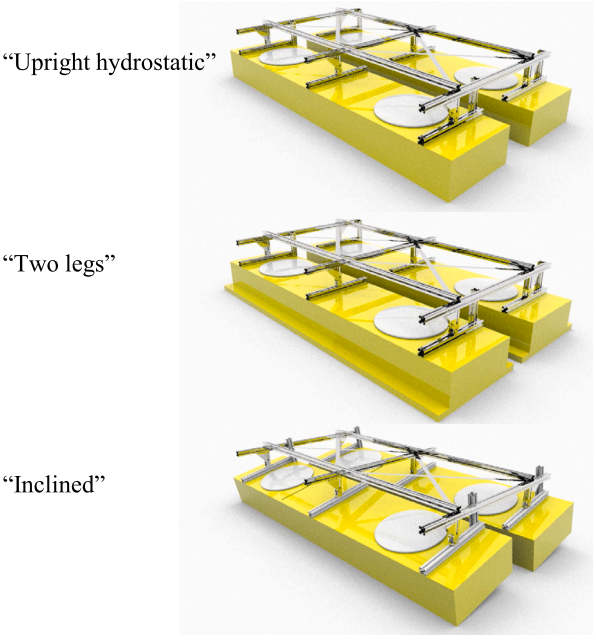

Fig. 2. Sectional model configurations.

1.6. Paper layout

This paper is divided into six sections that describe both physical research and numerical study. Sections 2 and 3 provide detailed explanations of the research design and applied methodology, and Section 4 presents both measured and calculated results. Furthermore, Section 5 provides additional information on other design topologies, calculated numerically, to extend the discussion presented in Section 6.

2. Physical testing

2.1. Testing program

The model was tested under 11 different wave periods of monochromatic waves, at an equal duration of 300 waves. The shortest wave period was 10 s and the longest was 15 s at full scale. That said, special attention was given to the periods around the 12 s where gap resonance was expected. The exact periods used in the testing program are given in Table 2 with the conversion between full and model scales. Fig. 3 shows the model in the towing tank with the aluminum cross-structure frame, data acquisition, and mooring arrangement.

2.2. Data acquisition

Two types of data sets were acquired during the physical testing: wave elevation and the motion response of the modules at six degrees of freedom. Wave elevations were measured using wave gauges before and after the area of the models, and motion responses were captured using an optical motion tracking system. The optical system and the acoustic wave gauge sensor (WG-4) samples at 100 Hz with analogue output signal read by data acquisition at 1000 Hz. The wire wave probes (WG-1 and WG-6) signals through a 100 Hz low-pass filter before data acquisition.

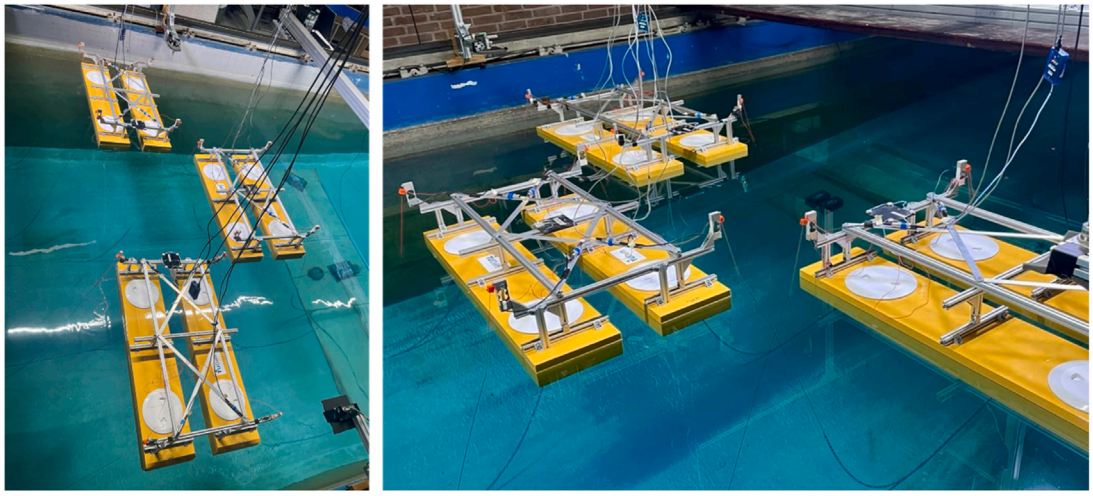

Fig. 3. "Scattered" + "Upright hydrostatic" configuration during an experiment run, showing also the composite mooring arrangement detailed in Sections 2.4 and 3.4.

Table 2
Tested conditions; regular wave periods T.

Full scale T (s):	10	11	11.5	11.75	12	12.25	12.5	12.75	13	14	15
Model scale T (s):	0.632	0.696	0.727	0.743	0.759	0.775	0.791	0.806	0.822	0.885	0.949

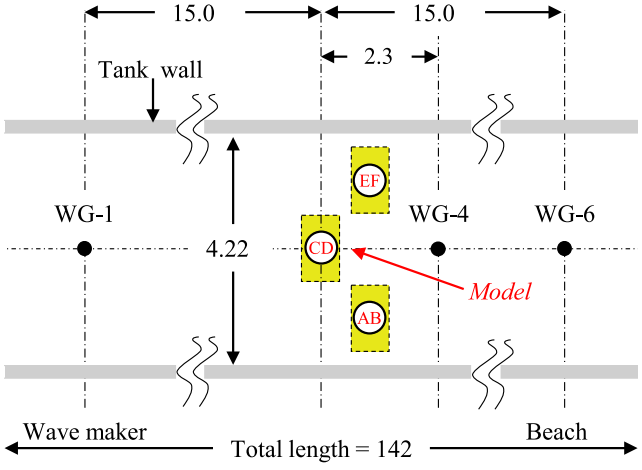

Fig. 4. Towing tank schematics and model position. Dimensions in meters.

2.3. Model design

Three equal modules were manufactured to carry out the experimental study based on the choice of design and the constraints outlined in Section 1.3. The hulls of the modules are made entirely of plywood and the cross-structure connection is made from aluminum ITEM profiles. The models were fabricated and equipped manually, resulting in small differences in the mass and inertia properties of the bare hulls. This was compensated during the ballasting of the models to the correct draft, so that all model particulars are identical within a margin of 5%. The project number assigned to these models is 538, and each hull received a letter notation from 'A' to 'F' and each module (made from two hulls) was registered under the project number and the two letters of the combined hulls (that is, 538 AB, 538 CD and 538 EF). As this is a 2D study, the results presented are based only on module 538 CD positioned in the middle (in the center line of the towing tank). The weight of the module tested is 59.06 kg, and the inertia about the x-axis (of the module) is 3.0 kg m^2.

2.4. Mooring design

During the physical experiment, each module was connected in the bow (starboard and portside) and in the stern (starboard and portside), with four mooring lines. The chosen mooring design allows the modules to move freely in the first-order motion response while maintaining a relative position from drift. The chosen mooring arrangement also reflects the applied mooring design in practice for the conditions in the North Sea and the Eastern Mediterranean Sea. In the tested model, the mooring arrangement includes a steel chain (diameter = 3 mm, length = 2 m, weight = 0.1595 kg/m), and a rigid nylon line. In the current setup, the non-linear spring reaction of the chain is intermediated with that of the floating model through the rigid nylon line, which is an order of magnitude stiffer than the catenary stiffness of the chain. This approach allows one to calculate beforehand the desired catenary stiffness, based on the expected horizontal drift forces obtained by the numerical model, using, in this case, the Near Field Solution method. Thus, the horizontal forces calculated analytically (Ma et al., 2019) can be matched to those obtained numerically to design the correct stiffness.

3. The numerical platform

There are two main reasons for developing numerical models together with physical tests. First, to optimize the physical model design as part of the test preparations, and second, to evaluate the physical results with the results obtained numerically. Thus, ensuring the readiness of the model's design for testing and then checking the ability of the numerical platform to simulate reality. To calculate the wave structure interaction of floating seawalls, a parametric boundary element model is programmed for the analysis system ANSYS-AQWA (2022R1), using MATLAB (R2022b) codes to generate the required preprocessing data files and postprocessing calculations. The data files (.dat) created in the preprocess codes encompass the entire model geometry (including the required characteristics such as mass, the center of gravity (COG), and inertia) and the environmental conditions (e.g., water depth, wave periods, and wave directions). The post-processing code reads back to MATLAB the output data file (.LIS), which is an ASCII file containing the model definition/analysis parameters and the analysis results, to be further analyzed.

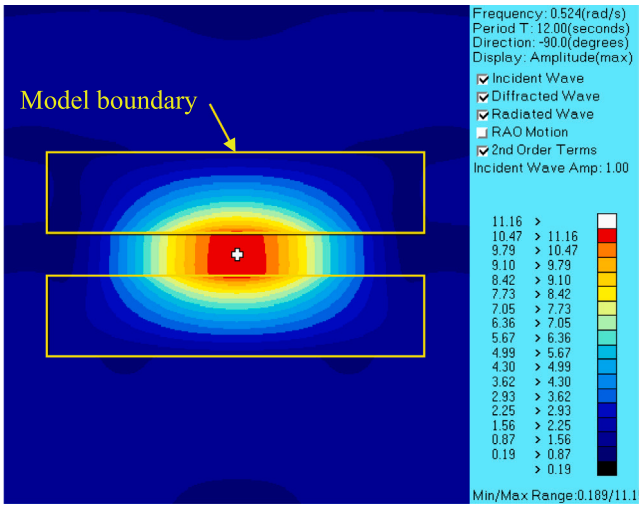

Fig. 5. Wave surface contours plotted with AQWA Graphical Supervisor (AGS).

ANSYS-AQWA is a potential flow theory solver, and as such, the assumptions are that the fluid is irrotational and incompressible, and the waves are of small elevation (Wehausen and Laitone, 1960). The MATLAB to ANSYS-AQWA model was verified by reconstructing the results presented by Ray (2000) for a simple box, calculated with both WAMIT and MOSES. Two widely used and well-proven 3D diffraction and radiation computer software. This validation was published in an earlier study (Wang et al., 2020b). Beyond this validation, the analysis system ANSYS-AQWA has been used in many published studies, exploring the hydrodynamics of wave-structure interaction and wave energy devices, and is considered an adequate and acceptable numerical tool (e.g., Drimer and Gafter, 2017; Jiang et al., 2021; López et al., 2017).

3.1. Limitations – vortex generation and gap resonance

The potential flow theory assumes inviscid flow and, as such, viscous drag is not considered in the solution provided. This is a known and discussed topic in the literature (e.g., Bhinder and Murphy, 2019). However, in real-world conditions, the response between two structures is often damped as a result of viscous effects that are not captured by the potential theory solver, which tends to over predict the amplitude of the response. A good example of this over prediction is vividly manifested at the response amplitudes to gap resonance at a specific wavelength as can be seen in Fig. 5. In this condition, the wave amplitude that accumulates in the gap between the hulls of the module reached about ca. 11 times the incident wave amplitude. Correlating this result with real-life conditions, at a peak period (T_p) of 12 s, and an estimated incident (significant) wave height (H_{m0}) of 4.8 m. The wave height developed in the gap between the modules exceeds 50 m. In any case, it is important to understand that although the numerical solver overestimates the wave elevation for that instant, it is very successful in capturing the phenomenon. Providing valuable input to the user, with a simple frequency sweep.

The relation between the peak period (T_p) in seconds and the significant wave height (H_{m0}) in meters, given in Eq. (2), is based on data measured by the Israeli Coastal and Marine Engineering Research Institute - CAMERI, over the last 30 years. The statistical data used from this relation consist of storm waves where (H_{m0}) is larger than 2 m.

$$T_p = 5.45\sqrt{H_{m0}} \tag{2}$$

The potential flow solver was selected for this study for its ability to analyze a wide range of wave frequencies over a large area (approximately 4 by 4 km). This is essential for computing the wave patterns on the leeward side of the seawall and determining the wave transmission coefficients. Furthermore, the solver can be adjusted to different sectional configurations ("Upright hydrostatics", "Two legs", and "Inclined"), draft, wave angle, and spatial arrangement without needing to reconstruct the domain and go through long convergence process. In comparison, running a similar domain with a viscous flow model would require much more computing power. Therefore, the current study does not provide a comprehensive analysis of the seawall configuration in the gap resonance region using a viscous flow model, and this is considered for future research.

3.2. Grid sensitivity

To solve a hydrodynamic problem in ANSYS-AQWA, only the wetted surface area of the model is considered and the number of diffraction panels is limited to the program memory allocation (ANSYS, 2022). In the analysis carried out in this study, the total number of diffraction panels was approximately 30,000. In the older version of the program, the number of diffraction elements was limited to only 12,000 (ANSYS, 2011), which is approximately the amount required for the modeling of one module. To determine whether this limitation decreases the quality of the results obtained, a numerical convergence study was performed to evaluate the sensitivity of the grid density (i.e. the number of boundary elements). In the current context, numeric convergence means that, when the mesh density increases, the numeric solution becomes closer to the real solution. However, because there is no real solution, the results can only be evaluated at different grid densities and compared with the maximum available diffraction elements in the software. ANSYS-AQWA also provides geometrical boundary rules for creating valid elements for computational considerations. For theoretical considerations, the element length (in the wave direction) should be less than 1/7 of the incident wavelength. And from numerical considerations, the elements should have an aspect ratio greater than 1/3, in addition to the fact that the center of the elements should be at least one equivalent radius apart from the elements (ANSYS, 2011). The definition of the aspect ratio (AR) is given in Eq. (3), where A is the plate element area, L is the longest side of the plate element and C is obtained from the relation given in Eq. (4), where n is the number of sides of the element. And Eq. (5) shows the equivalent radius (Re) relation also known as the facet radius.

$$AR = \frac{A}{L^2}C \tag{3}$$

$$C = \frac{4}{n\tan(\frac{90-360}{2\pi})} \tag{4}$$

$$Re = \sqrt{\frac{A}{\pi}} \tag{5}$$

For the mesh convergence study, a single pontoon model was created in ANSYS-AQWA and 13 different grid densities were examined. Starting at 20% grid density (with 2580 boundary elements), and gradually increasing the resolution (by changing the number of nodes) to 100% grid density (with 11988 boundary elements). The 13 grid models were calculated under the same conditions using five different wave periods: 6, 8, 10, 12, and 14 s — in deep water, where the depth of water is greater than half the wavelength.

To review the performance of the different densities of the grid, an evaluation of the hydrodynamic coefficients (added mass and damping) was performed. The results of all 13 models were evaluated; however, no convergence trend was found. Therefore, by programming the grid density in accordance with both theoretical and numerical computational considerations, the results tend to be sufficient — without evidence of a significant improvement when the number of elements increases. Similar conclusions to this can be found in other studies using ANSYS-AQWA (Ma et al., 2020; Masoudi and Gan, 2021; Penalba et al., 2017; Subbulakshmi and Sundaravadivelu, 2021). In other published studies, also using ANSYS-AQWA, the mesh size is not discussed or reported (e.g. Chen et al., 2017; Yeh et al., 2021).

The evaluation of hydrodynamic coefficients (added mass and damping) provides a view of the grid size sensitivity with respect to the hydrodynamics of the structure. However, the current research examines also the transmission wave heights at the leeward side of the structure. Thus, the wave field on the leeward side of all 13 models was also examined. For each model, a total of three waypoints were defined, at the leeward side, and wave elevation was measured using the AQWA Graphical Supervisor (AGS). The waypoints were located 200, 500, and 1,000 m from the centerline of the module. Also, here, the quality of the obtained results did not significantly improve (or converge) when the number of elements increased.

3.3. The towing tank walls

The effects of the towing tank walls (as shown in the schematics in Fig. 6) on the measured results are examined to help improve the agreement between the physical experiment and the numerical results. It is assumed that if the results of the numerical model are closer to those obtained in the physical experiment (with side walls), it will increase the overall confidence in the numerical platform. The side walls of the tank are added to the boundary element model (BEM) as a fixed structure (diffraction elements). The length of each side wall is 3,000 m, at full scale and 12 m on model scale. The depth of the water of the towing tank is 2.3 m, which corresponds to a depth of the seabed of 575 m in the full scale, and the fixed wall structure extends all the way to the towing tank floor (or seabed). In the BEM model the wall is one-element wide, which is 22.0 m at full scale and 9.0 cm at model scale. Therefore, the distance between the floating module tested (that is, the center of gravity of the CD module (Fig. 4) and the edge of the wall, in the longitudinal direction, is 1500 m.

3.4. Moorings analysis in time domain

To include the impact of the mooring arrangements (detailed in 2) on the numerically calculated structural response, additional analysis is performed in AWQA-NAUT. This is a time-domain program that uses the hydrodynamic coefficients calculated initially in the frequency domain by AQWA-LINE. Using Froude scaling laws, the numerical mooring arrangement (in full scale) is based on the physical mooring setup for both dimensions (position and length) and catenary stiffness (as a function of the uniform mass per unit length (kg/m) and the unstretched mooring line length). The following data input is used in AQWA-NAUT to define the composite mooring arrangement: the steel chain length is 500 m and the mass per unit length is 1.09E04, the rigid nylon line is 465 m and the mass per unit length is 6.20E01. The time-domain analysis is performed in monochromatic waves to match the conditions of the physical experiment.

Despite the fact that the compliant mooring system has been fully detailed in the presented analysis, it is not considered an active measure to increase wave absorption, but rather an additional facility to increase the similarity between experimental and numerical setups. Mainly, with respect to the second-order drift force effect and the associated module position.

3.5. Image processing for wave elevations

The interpretation of the wave elevations calculated by the solver is key to providing a good comparison with the results tested in the towing tank. As reported in Section 2, the acquisition of wave elevation data is obtained by wave gauges placed before and after the tested model. The same positions have been used on the numerical platform to extract the pin-pointed data. However, as the binary Velocities at Centroids file (.VAC) created by ANSYS-AQWA cannot be decoded by the software users, an image processing code written in MATLAB was used to generate the elevation values. This code interprets the images of the wave surface contours created by the graphical supervisor (AGS)

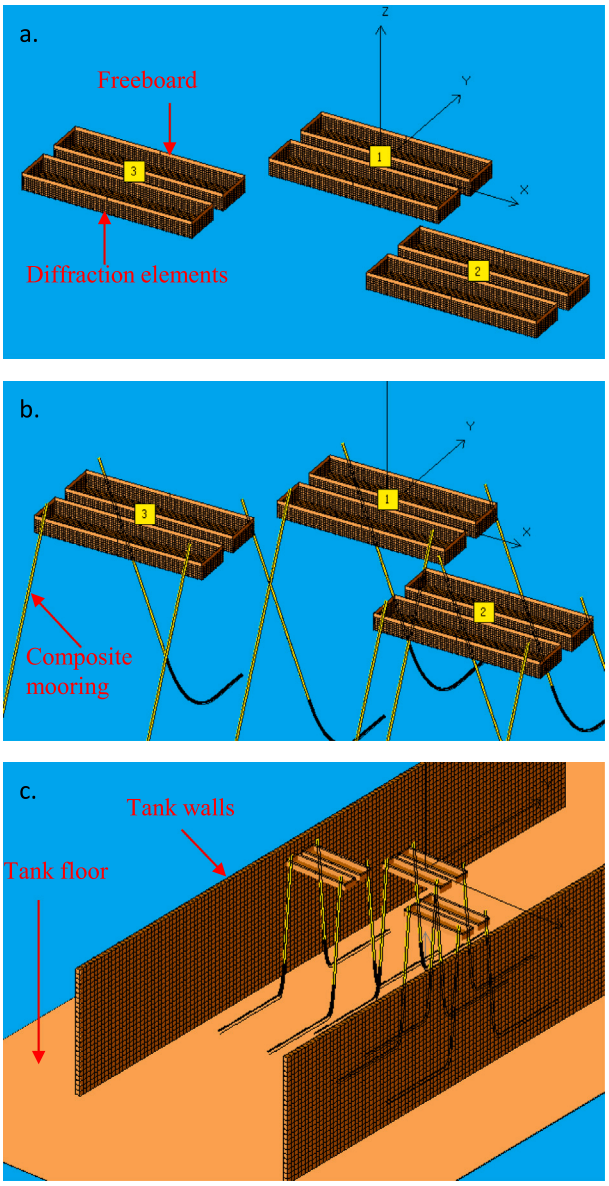

Fig. 6. a. principal model geometry for AQWA-LINE, b. including composite mooring (AQWA-LIBRIUM), c. the complete model including fixed walls structure, tank floor and moorings (AQWA-NAUT).

in ANSYS-AQWA since a more direct approach was not found to use the mathematical data.

A typical investigation data segment was considered to calculate the average wave field behind the seawall for each wave period. This location is considered a sheltered area for the implementation of ocean and sea space utilization projects in open water conditions. The data segment is located in the same position as the leeward wave gauge (WG-4) in the physical test setup (shown in Fig. 4). The size of the data segment in the numerical analysis is 350 by 168 m, and the distance from the center of the middle module is 575 m. On the model scale, the measured footprint is 0.94 m2 and is located 2.3 m behind the middle module. Several attempts were made to find the correct area for the data segment, by correlating the numerical results with the measured transmitted wave height (outside the region of resonance) before choosing the analyzed image process data segment outlined above.

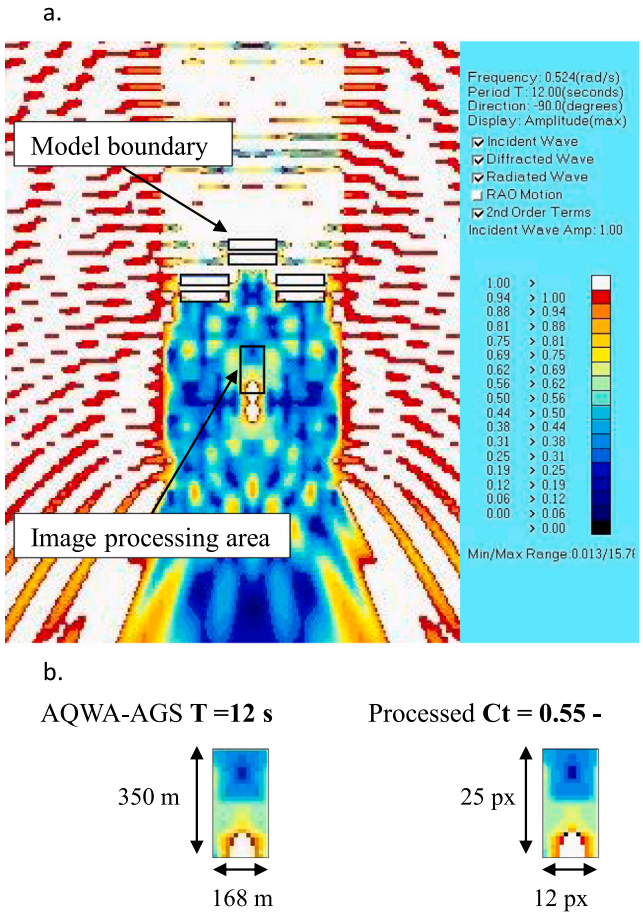

Fig. 7. a. wave surface contours plotted with AQWA Graphical Supervisor (AGS) at 12 s wave periods, b. The analyzed image process data segment.

Since the incident wave height in ANSYS-AQWA is always 1.0, the projected wave surface contour values indicate the transmission coefficients obtained with respect to the incident wave values. Therefore, the color code scale already provides the transmitted wave coefficients (given in Eq. (1)). As this is an automatic process, it has the capacity to sweep over a large number of frequencies, in a short time, and to examine whatever resolution (the size of analysis area) to compare with the results obtained in the physical testing or other.

Fig. 7 shows the principal image processing code for a wave period of 12 s. Part a. shows the wave field generated by AQWA-AGS, where the image processing area and the model boundary are indicated. In part b. the image processing area is given as a cut out of the AQWA-AGS file together with the color-coded MATLAB values (where the dimensions are given in pixels). To calculate the average amplitude of the image process area in MATLAB, the amplitude scale (rainbow scale) is used to set color-coded values. In this analysis, all amplitudes greater than 1.00 have been omitted and the ruler scale values are between 0 and 1, with a gradient of 18 steps.

4. Results

The results presented in this section focus on the response amplitudes and the performance of the floating seawall. Here, the agreement between the numerical values and the measured experimental data is also evaluated on this basis. First, the results of the physical experiment with respect to the response amplitudes of the middle module (module CD as shown in Fig. 4) are examined against the values obtained numerically. Then, the effectiveness of the proposed floating seawall concept is evaluated using the calculated transmission coefficients (given in Eq. (1)) using both physical data sets and numerical results.

4.1. Measured wave elevations

During physical experiments the wave heights are measured, using wave gauges located before and after the model, to calculate both the structural response and transmission coefficients. The measured signals (containing approximately 300 waves) are partially contaminated by reflections from the walls of the tank and the beach. Therefore, it is necessary to capture a relatively clean and representative segment of these signals to describe the intended conditions. To do so, each signal is Fourier-transformed via FFT (frequency spectrum) to filter unwanted frequencies, and then a fit function is used to return a clean signal. The selected time series for WG-1 is mainly motivated by a steady clean signal (early in the measurements), and WG-4 aimed to capture the same wave train (measured earlier with WG-1) at the leeward side of the model. Data collected from WG-6, positioned 15 m behind the model (or 3750 m on full scale), were not used to calculate the transmission coefficient, as it was too far behind and misrepresented the measured values with relation to floating seawall performance.

The two data sets measured from WG-1 (incident wave) and WG-4 (transmitted wave) were initially used to calculate the response of the structure to the unit wave amplitude and the transmission coefficient (C_t). However, due to the accuracy tolerance of the wave gauges and the small propagated wave amplitudes (from 2.5 to 9.3 mm) designed for the experiment (at a scale factor of 1:250), the results obtained using this methodology were inadequate. In addition, WG-1 is a resistive wave level probe and WG-4 is an acoustic wave gauge, and although they are fully calibrated, the smallest embedded difference can affect the obtained result in the current testing resolution. To overcome this limitation, the incident wave and transmitted wave heights are taken only from WG-4. Where the incident waves are taken from the measurements runs without the model, and the transmitted waves are taken from the measurements runs with the model.

4.2. Response amplitudes

In the physical testing, the motion responses, in six degrees of freedom, are captured using an optical motion tracking system with a reference plate on each model. The location of the reference plate is measured and transformed to the frame of reference to show the values about the center of gravity. The obtained results, with a sample rate of 1000 Hz. are Fourier transformed in a similar way to the process outlined in the previous section.

In addition to data acquisition from the physical testing, the results presented in this section show the structure response (amplitudes) per unit wave at the relevant degrees of freedom (sway (y), heave (z) and roll (rx)) of the numerical model as well. Fig. 8 shows the results obtained by both the physical test and the numerical platform. The response amplitudes obtained numerically are calculated with AQWA-NAUT, a non-linear time domain analysis that includes the mooring constraint, as shown in 6.

The principal ANSYS-AQWA values are obtained from the relation shown in Eq. (6) when writing $X = X_0 e^{-i\omega t}$ and $F = F_0 e^{-i\omega t}$. Where X is the motion amplitude, M_S is the mass of the structure, M_A is the added mass (frequency dependent), C is the hydrodynamic damping (frequency dependent), and K is the hydrostatic spring. For multiple bodies, say N, this relation is extended so that X and F are now vectors of size $6N \times 1$ and the coefficient matrices (M_s, M_A, C, K) are of size $6N \times 6N$. All interactions between bodies are then incorporated into the coefficient matrices.

$$[-\omega(M_s + M_A(\omega)) - i\omega C(\omega) + K]X(\omega) = F(\omega) \quad (6)$$

AQWA-NAUT solves the second-order differential equations of motion for each structure, integrating them to form a time–history. For this, the program requires the initial conditions (the above-mentioned frequency response of the structure)in order to begin the integration. A time history of the wave frequency response can be found by combining the response amplitude operators with the corresponding wave frequency (ANSYS, 2011). This is done for each degree of freedom as shown in Eq. (7):

$$-x(t) = aXe^{i\omega t + ikx_p} \tag{7}$$

where, X is the complex response amplitude at wave frequency ω, ω = the frequency of the component of the regular wave, k = the wave number corresponding to the frequency of the wave ω, x_p = the distance from the origin of the wave system perpendicular to the direction of the wave, a = the amplitude of the component of the regular wave and $x(t)$ = the instantaneous displacement at time t.

The results for the time domain (AQWA-NAUT) and the physical tests are processed in a similar way. The response amplitudes of the center module (CD) are divided by the incident wave amplitudes. The incident wave amplitudes outlined in Section 4.1 are used in the physical testing and the input incident wave amplitude of 1.0 is used in the numerical model.

The response amplitudes presented in Fig. 8, provide an interesting view of the compliance of the numerical model with physical tests. Knowing the limitation of the numerical analysis (see Section 3.1), it is logical to obtain some differences. However, the results show good agreement between AQWA-NAUT and the physical tests in the area outside the gap resonance. The sway (y) and roll (rx) show very good agreement up to a wave period of 13 s, then at 14 s there is a slightly larger difference, which reduces again at 15 s. The response amplitude in Heave (z) also shows very good agreement up to 12 s, where the gap resonance peaks, and the numerical results are predictably exaggerated (as shown in Fig. 5), from 12.5 s to 14 s, in the absence of the gap resonance, a good agreement between the numerical and physical results is maintained. In a wave period of 15 s, a relatively larger difference is observed.

4.3. Wave transmission coefficient (C_t)

For the numerical model, the transmission coefficient (C_t) is calculated based on the results obtained from the wave contours (AQWA-AGS), which are calculated in the frequency domain. The calculation process is presented in Section 3, in image processing for wave elevations. The transmission coefficients (C_t) for the physical tests are based on the incident wave and transmitted wave heights measured and processed from WG-4.

The results presented in Fig. 9 show the calculated C_t of the numerical and physical models. The results show good agreement in the wave periods before and after the area considered influenced by the gap resonance at around the wave period of 12 s. Naturally, the measurement error increases at short-wave periods, where the amplitudes are relatively smaller. However, in the periods where gap resonance occurs, we see the opposite behavior between the physical tests and the numerical results. The numerical results show a significant decrease in the floating seawall performance between 12 and 13 s, while the measured values show a significant improvement.

5. Module topologies, draft, and arrangements

This section provides an opportunity to evaluate additional topologies for existing ships, in order to transform them into more efficient modules in a floating seawall arrangement. The result in this section presents the transmission coefficients for each typology tested, using the numerical tools described and developed throughout this paper. On the basis of the evaluation between the results calculated numerically and the physical tests, we already know that at wave periods where gap resonance takes effect, the results might be the opposite. Where the measured values show significant improvement as opposed to the numerical results. With this knowledge installed, the values obtained numerically in the previous section are considered as the main benchmark to the results presented hereafter.

5.1. Change of draft

This section evaluates the performance of the seawall as a function of its draft. In real life, existing vessels, intended to be used as floating seawall modules, are designed and constructed with a limiting operational draft. This draft is chosen with respect to the heaviest loading condition (commonly, when the vessel is fully loaded prior to departure), and relates primarily to the stability of the ship (e.g., hydrostatics and range of positive stability), and its structural integrity (e.g., sufficient safety factors in longitudinal bending conditions), in compliance with regulatory codes. However, when recommissioning these vessels to act as a floating seawall module, classification notation is changed (if at all applicable…) and the draft can be assumed other than its previous maximum, to improve the wave attenuation capacity. In this study, the chosen ship already has an extreme draft-length ratio, and the physical tests concentrate only on that. However, the numerical platform enables further examination of the impact of the draft, for a better understanding of the trade-offs between structural compliance and wave attenuation performance.

The change in the draft of the vessel can have an impact on the wave attenuation performance, without the complication of morphological change in the existing hull. The results presented in this section show the variation in wave attenuation capacity based on the different loading conditions. Four additional loading conditions are examined for the same model, in draft changes of 2 m intervals from 15 m to design draft (T = 23 m). The inertia moments for each loading condition are calculated in relation to the newly obtained displacement associated with the change of draft. The numerical results, presented in Fig. 10, show the transmission coefficients for the various drafts at the same wave periods used in the previous experiment.

The influence of the draft on the wave attenuation is evident, and generally the increase in the draft improves the wave attenuation performance. However, at wave periods closer to the gap resonance, the behavior is much less stable. It becomes more settled at wave periods from 13 to 15 s, where the decrease of the transmission coefficient is almost linear to the change of draft. Furthermore, at a wave period of 11 s, T = 21 m has a lower transmission coefficient than T = 23 m.

5.2. Cross sections

As reported earlier, the current research investigates three types of cross section: (1) upright hydrostatic at the design water line, (2) two legs retrofitted with an external structure, and (3) inclined configuration at the deck immersion point (at heeling angle of 12°). The upright hydrostatic configuration has been tested and presented in the previous sections. Thus, this section will incorporate additional results on the already collected benchmark data. The external structure refers to the rectangular two-legged floating breakwater introduced in the Introduction in Sections 1.4 and 1.5. Although it requires additional resources in terms of implementation (refitting the two legs), it promises to contribute to wave attenuation. The cross-sectional dimensions of each additional structure are 4 by 4 m and extend throughout the length of the module, as shown schematically in Fig. 2. However, the inclined position requires no structural intervention and can simply be achieved by introducing a weight shift.

In Fig. 11 it is evident that the cross-sectional modification has a large impact on the leeward wave characteristics calculated with AQWA-LINE. The two-leg configuration increases the performance of the seawall in wave periods of 11 to 14 s. However, the influence of the gap resonance is not as prominent and therefore in real life the

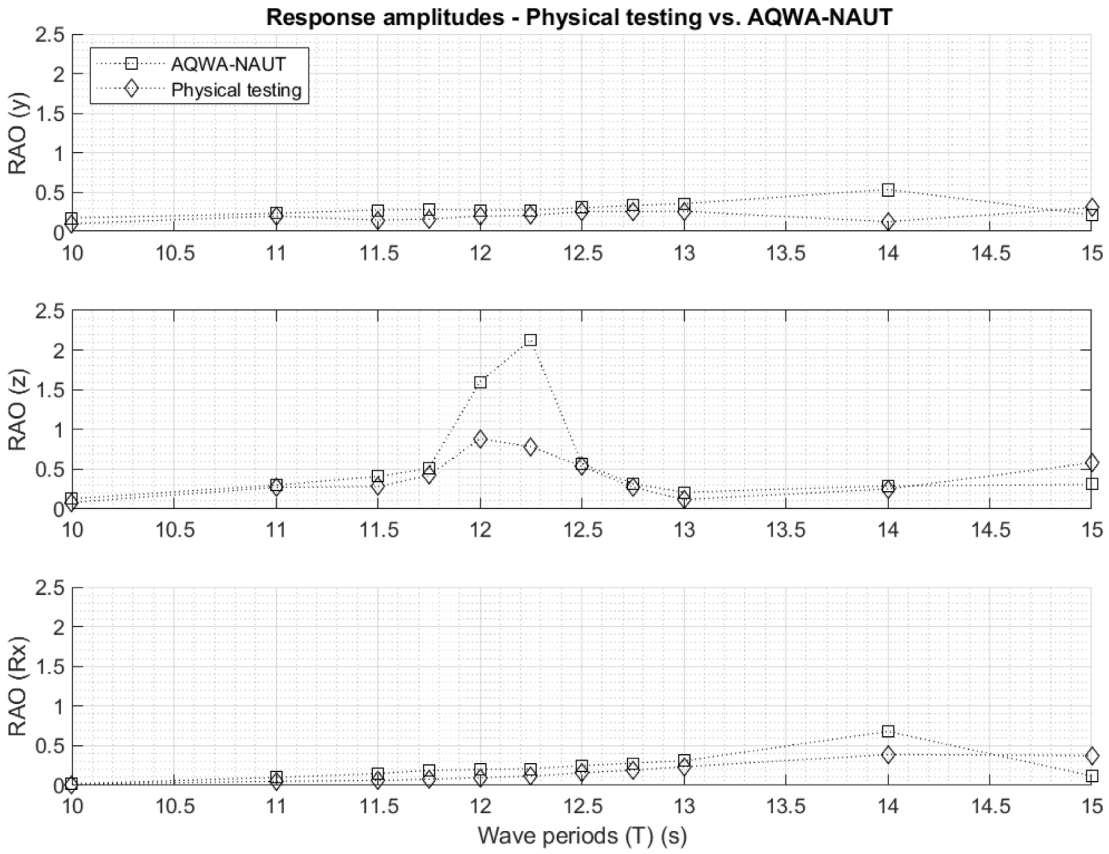

Fig. 8. Response amplitudes per unit wave.

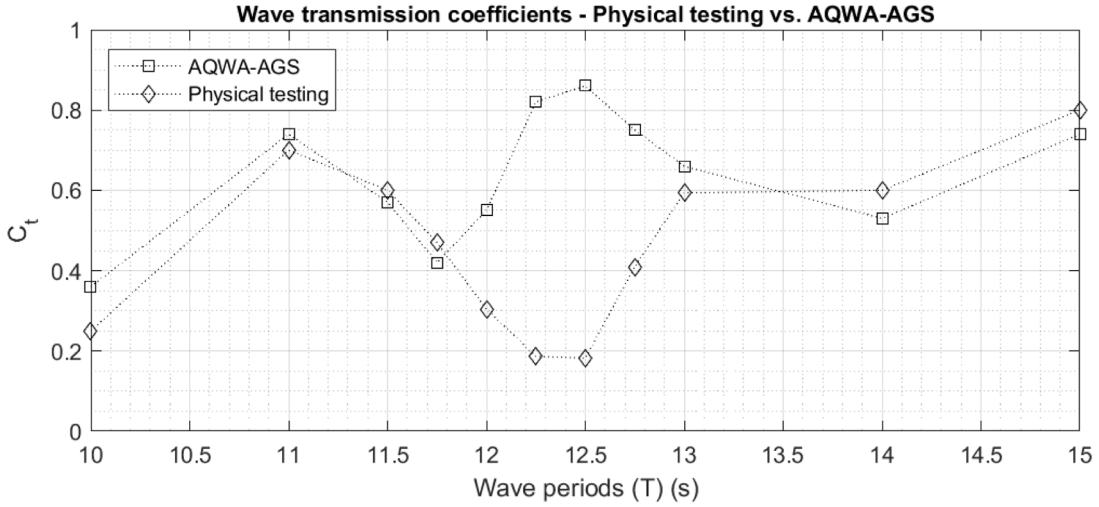

Fig. 9. Evaluation of numerical and physical tested transmission coefficients values.

upright hydrostatic could provide better values between 12 to 13 s wave periods (as shown in the physical testing in Fig. 9. The inclined configuration provides the best results for wave periods between 12 to 15 s, with a steady transmission coefficient around $C_t = 0.2$.

6. Discussion and conclusions

A novel design for a floating seawall, made entirely of end-of-life oceangoing vessels was presented in this study. This concept has been developed and evaluated using both experimental and numerical tools, including the development of procedures for the automatic analysis of numerical results for different models. One of the major design features, in addition to the reuse of existing ships, is the induced gap resonance at 12 s periods to contribute to the performance of the floating seawall. This chapter will review the results presented in this paper and draw the necessary conclusions.

6.1. Gap resonance

The associated effects of gap resonance on the wave attenuation capacity of floating seawalls in a twin-hull configuration were tested for 12 s wave periods. The experimental result was consistent with

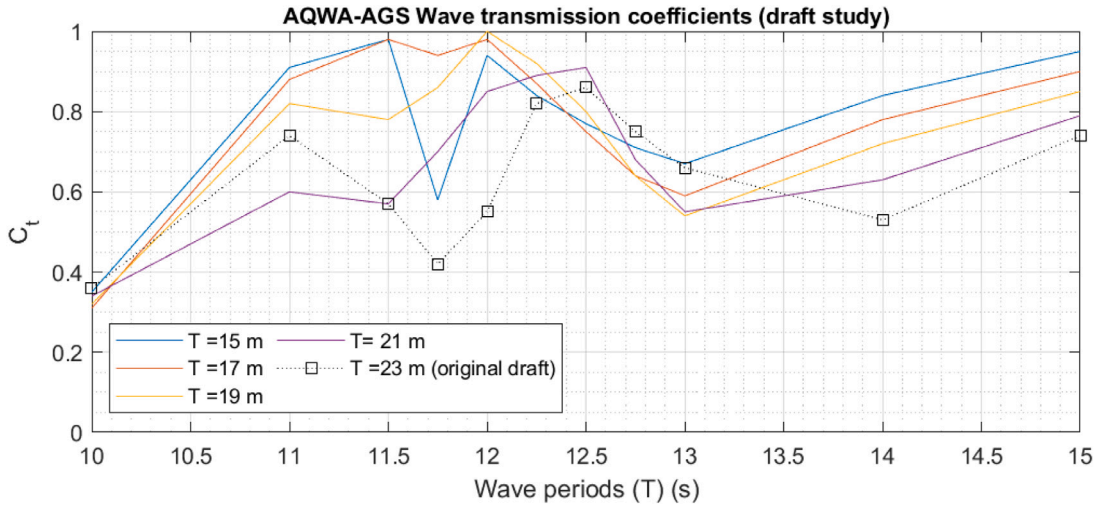

Fig. 10. Numerical transmission coefficients as function of the modules' draft (T).

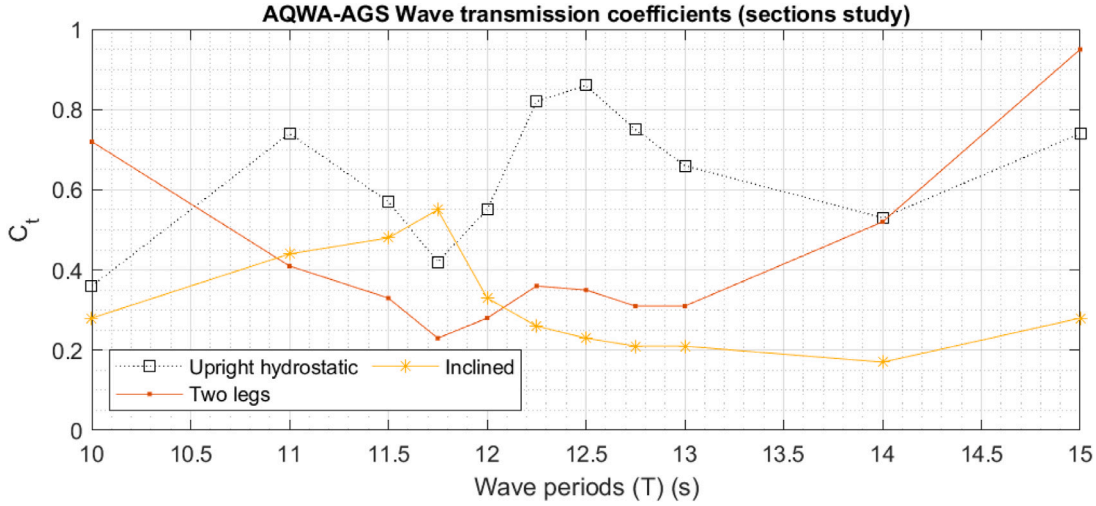

Fig. 11. Numerical transmission coefficients with additional cross sectional configurations (Two legs and Inclined).

the phenomenon predicted by the potential flow solver with great precision for the resonance incident, as shown in Fig. 5. From the results presented in Fig. 9, it is clear that the effect of gap resonance on the transmission coefficient obtained numerically is the opposite to that obtained by the physical model. The numerical solution is based on the 'wetted' geometry modeled in the flow domain, where everything above the waterline is assumed, and is represented primarily through the weight properties and the moment of inertia. The 400,000 DWT bulk carrier vessel was designed with a very limited freeboard (7 m in full scale and only 28 mm in model scale), under full loading conditions, which also influenced the result of the gap resonance and the large differences obtained between the numerical and physical testing. The standing wave between the hulls of the module could not accumulate to larger amplitudes before 'overtopping' the weather deck of the module, different from the numerical solution where the amplitude of the standing wave at 12 s is 11 times the incident wave amplitude (shown in Fig. 5). Although the principal properties (weight and inertia) are equal, the part above the water appears to have a great influence on the experimental results, since the effect of green water washing over the weather deck in the region of the gap resonance is not considered in the solution of the numerical model.

The results presented in this study are very supportive of the design and implementation of the floating seawall concept. First, the wave attenuation, based on the physical model, is very promising in the area of gap resonance. This decreases the incident wave by 80%. Second, the numerical platform is able to calculate the exact occurrence of a gap resonance based on the geometry and chosen wave periods, giving the user the ability to design accordingly. Harnessing the characteristics of gap resonance to floating seawalls is encouraged in future research to better understand this phenomenon in different shapes and configurations. Furthermore, gap resonance could also be explored in the context of wave-harnessing devices, as standing waves can be created and amplified using the geometry of the floating device. For example, a wall-sided hull and large freeboard are assumed to help increase the amplitude of the standing wave.

6.2. *Transmission coefficient*

Calculating and measuring the wave transmission coefficient is one of the main goals of this study. However, it has been a real challenge to capture the characteristics of the wave attenuation using pinpointed data measured by wave gauges or analyzed analytically in the numerical solver. The challenge was even greater to find a good agreement

between the tested and the calculated data. For that reason, we have chosen to broaden our measuring scope (calculated wave segment) on the numerical platform as explained in Section 3. Extending the image processing area, as shown in Fig. 7, we were able to obtain an adequate agreement between physical and numerical data outside the area influenced by the gap resonance. This had given us an overall confidence in the evaluation method and the results obtained – also in the region of the gap resonance – where the difference was expected. The main conclusions drawn from this study, with respect to the transmission coefficient, are: (1) Based on physical testing, we can conclude that the gap resonance between the two rigidly connected hulls helps to improve the transmission coefficient characteristics. (2) Based on the numerical solver, we can conclude that the inclined configuration of the two rigidly connected hulls contributes significantly to the transmission coefficient with respect to the normal upright hydrostatic (without heel or trim).

6.3. Configuration, draft, sections study

This research has focused on one spatial configuration: "Scattered". Scattered configuration is the preferred option from a structural perspective as the modules are not connected and the risks associated with connection failure and fatigue, mainly in extreme conditions, are lower. Additionally, it requires less effort (both financial and energy) to convert existing ships into seawall modules. The draft study has shown a significant wave reduction only at long wave periods. Thus, increasing the draft to improve wave attenuation should be examined in relation to the dimensions of the modules and the anticipated wavelength under local environmental conditions.

As already mentioned in the previous section, the cross-sectional study provided important input for the design of future floating seawalls constructed from end-of-life oceangoing vessels. First, the numerical results show agreement between the approach suggested in the scientific literature with respect to the effect of the additional structure ('Two legs') on the transmission coefficient. Furthermore, the inclined position provided a significant improvement to the transmitted wave coefficient due to the increase in beam and depth. The results of the inclined configuration are particularly interesting, as this modification does not require additional structure or massive refit. It only requires a change of weights from the centerline.

When designed correctly, floating seawalls can drastically reduce the amount of waves that pass through them, allowing the construction of floating structures even in the most extreme and challenging coastal environments.

7. Future research

7.1. Spatial arrangements

The potential of using end-of-life ships as a floating seawall has been the focus of the current study. However, the investigation referred to one specific spatial layout, as explained in Section 1.5. To further examine the wave absorption characteristics of the proposed module, additional configuration should be explored in future research. Providing parametric spatial optimization based on their spacing, alignment, and orientation.

7.2. Viscous flow model and artificial damping lid

The purpose of the current research is to evaluate the wave attenuation capacity of the proposed floating seawall to incoming beam waves, where the area gap resonance occurs, a particular point of interest due to the assumed energy dissipation. However, this study does not suggest or encourage the use of the potential flow solver to accurately simulate the physical phenomenon of gap resonance. On the contrary, it highlights the limitations of the solver to deal with the gap resonance, while providing good agreement to the experimental results outside that area. Therefore, to provide a complete numerical solution across the entire frequency range, the importance of viscosity and nonlinearity of the fluid in the gap resonance problem should be addressed with a separate viscous flow model In future research, the use of the potential flow model theory for the entire frequency range and the viscous flow model only in the gap resonance region could help reconcile the differences obtained in the transmission coefficient between the potential flow solution and the physical tests presented in Fig. 9. Furthermore, this methodology could be an economical approach to implement a viscous flow model without exacerbating the need for a lot of computational resources. In addition to the viscus flow model, artificial damping lid method could be implemented using the data measured from physical testing in future research.

CRediT authorship contribution statement

Gil Wang: Writing – review & editing, Writing – original draft, Visualization, Validation, Software, Resources, Project administration, Methodology, Investigation, Funding acquisition, Formal analysis, Data curation, Conceptualization. **Daniel Bar:** Software. **Sebastian Schreier:** Supervision.

Declaration of competing interest

The authors declare that they have no known competing financial interests or personal relationships that could have appeared to influence the work reported in this paper.

Data availability

No data was used for the research described in the article.

Acknowledgments

This work was supported by the Israel Ports Development and Assets Company Ltd. and CAMERI - The Israeli Coastal and Marine Engineering Research Institute Ltd. www.cameri-eng.com.

References

Anon, 2007. Very Large Floating Structures. In: Wang, C.M., Watanabe, E., Utsunomiya, T. (Eds.), CRC Press, London ; New York.

ANSYS, 2011. AQWA ™-LINE MANUAL. Technical Report, ANSYS, Inc., United Kingdom.

ANSYS, 2022. Aqwa Reference Manual. (Release 2022 R1), Canonsburg U.S.A.

Bhinder, M.A., Murphy, J., 2019. Evaluation of the Viscous Drag for a Domed Cylindrical Moored Wave Energy Converter. J. Marine Sci. Eng. 7 (4), 120. http://dx.doi.org/10.3390/jmse7040120, URL https://www.mdpi.com/2077-1312/7/4/120, Number: 4 Publisher: Multidisciplinary Digital Publishing Institute.

Carr, J.H., 1951. MOBILE BREAKWATERS. Coastal Eng. Proc. (2), 25. http://dx.doi.org/10.9753/icce.v2.25, URL https://icce-ojs-tamu.tdl.org/icce/index.php/icce/article/view/1496, Number: 2.

Chen, X., Miao, Y., Tang, X., Liu, J., 2017. Numerical and experimental analysis of a moored pontoon under regular wave in water of finite depth. Ships Offshore Struct. 12 (3), 412–423. http://dx.doi.org/10.1080/17445302.2016.1172831, Publisher: Taylor & Francis _eprint:.

Dai, J., Wang, C.M., Utsunomiya, T., Duan, W., 2018. Review of recent research and developments on floating breakwaters. Ocean Eng. 158, 132–151. http://dx.doi.org/10.1016/j.oceaneng.2018.03.083, URL https://www.sciencedirect.com/science/article/pii/S0029801818303652.

Drimer, N., Agnon, Y., Stiassnie, M., 1992. A simplified analytical model for a floating breakwater in water of finite depth. Appl. Ocean Res. 14 (1), 33–41. http://dx.doi.org/10.1016/0141-1187(92)90005-5, URL http://www.sciencedirect.com/science/article/pii/0141118792900055.

Drimer, N., Gafter, R., 2017. Delta-type VLFS – hydrodynamic aspects. Ships Offshore Struct. 1–14. http://dx.doi.org/10.1080/17445302.2017.1384440.

Gao, J., Chen, H., Zang, J., Chen, L., Wang, G., Zhu, Y., 2020. Numerical investigations of gap resonance excited by focused transient wave groups. Ocean Eng. 212, 107628. http://dx.doi.org/10.1016/j.oceaneng.2020.107628, URL https://www.sciencedirect.com/science/article/pii/S0029801820306296.

Gao, J., He, Z., Huang, X., Liu, Q., Zang, J., Wang, G., 2021. Effects of free heave motion on wave resonance inside a narrow gap between two boxes under wave actions. Ocean Eng. 224, 108753. http://dx.doi.org/10.1016/j.oceaneng.2021.108753, URL https://www.sciencedirect.com/science/article/pii/S0029801821001888.

Gao, J.-l., Lyu, J., Wang, J.-h., Zhang, J., Liu, Q., Zang, J., Zou, T., 2022. Study on Transient Gap Resonance with Consideration of the Motion of Floating Body. China Ocean Eng. 36 (6), 994–1006. http://dx.doi.org/10.1007/s13344-022-0087-7.

Gao, J., Zang, J., Chen, L., Chen, Q., Ding, H., Liu, Y., 2019. On hydrodynamic characteristics of gap resonance between two fixed bodies in close proximity. Ocean Eng. 173, 28–44. http://dx.doi.org/10.1016/j.oceaneng.2018.12.052, URL https://www.sciencedirect.com/science/article/pii/S0029801818317244.

Gesraha, M.R., 2006. Analysis of *Pi* shaped floating breakwater in oblique waves: I. Impervious rigid wave boards. Appl. Ocean Res. 28 (5), 327–338. http://dx.doi.org/10.1016/j.apor.2007.01.002, URL https://www.sciencedirect.com/science/article/pii/S0141118707000041.

Glavovic, B., Dawson, R., Chow, W., Garschagen, M., Haasnoot, M., Singh, C., Thomas, A., 2022. Cross-Chapter Paper 2: Cities and Settlements by the Se. In: Climate Change 2022: Impacts, Adaptation and Vulnerability. Contribution of Working Group II To the Sixth Assessment Report of the Intergovernmental Panel on Climate Change. Cambridge University Press, Cambridge, UK and New York, USA, pp. 2163–2194, URL https://www.ipcc.ch/report/ar6/wg2/downloads/report/IPCC_AR6_WGII_CCP2.pdf.

Gong, S.-k., Gao, J.-l., Mao, H.-f., 2023. Investigations on Fluid Resonance Within a Narrow Gap Formed by Two Fixed Bodies with Varying Breadth Ratios. China Ocean Eng. 37 (6), 962–974. http://dx.doi.org/10.1007/s13344-023-0080-9.

Hartcup, G., 2006. Code Name Mulberry. Pen and Sword, Google-Books-ID 57XNDwAAQBAJ.

He, Z.-w., Gao, J.-l., Shi, H.-b., Zang, J., Chen, H.-z., Liu, Q., 2022. Investigation on Effects of Vertical Degree of Freedom on Gap Resonance Between Two Side-by-Side Boxes Under Wave Actions. China Ocean Eng. 36 (3), 403–412. http://dx.doi.org/10.1007/s13344-022-0036-5.

Huijsmans, R.H.M., Pinkster, J.A., de Wilde, J.J., 2001. Diffraction and Radiation of Waves Around Side-by-Side Moored Vessels. In: TUDelft, Faculty of Marine Technology, Ship Hydromechanics Laboratory Report 1300-P, Published in: The Proceedings of the International Offshore and Polar Engineering Conference, ISOPE2001, Stavanger, Norway, 17-22 June 2001, ISBN: 1-880653-51-6. URL https://repository.tudelft.nl/islandora/object/uuid%3Ac28eb1c1-edfd-4df1-92b0-4294485d440a.

Jain, K.P., Pruyn, J.F.J., Hopman, J.J., 2017. Material flow analysis (MFA) as a tool to improve ship recycling. Ocean Eng. 130, 674–683. http://dx.doi.org/10.1016/j.oceaneng.2016.11.036, URL https://www.sciencedirect.com/science/article/pii/S002980181630539X.

Jiang, C., el Moctar, O., Schellin, T.E., 2021. Hydrodynamic Sensitivity of Moored and Articulated Multibody Offshore Structures in Waves. J. Marine Sci. Eng. 9 (9), 1028. http://dx.doi.org/10.3390/jmse9091028, URL https://www.mdpi.com/2077-1312/9/9/1028, Number: 9 Publisher: Multidisciplinary Digital Publishing Institute.

Koraim, A.S., Rageh, O.S., 2014. Effect of under connected plates on the hydrodynamic efficiency of the floating breakwater. China Ocean Eng. 28 (3), 349–362. http://dx.doi.org/10.1007/s13344-014-0028-1, URL http://link.springer.com/10.1007/s13344-014-0028-1.

Lamas-Pardo, M., Iglesias, G., Carral, L., 2015. A review of Very Large Floating Structures (VLFS) for coastal and offshore uses. Ocean Eng. 109, 677–690. http://dx.doi.org/10.1016/j.oceaneng.2015.09.012, URL http://www.sciencedirect.com/science/article/pii/S0029801815004783.

Lavidas, G., Polinder, H., 2019. North Sea Wave Database (NSWD) and the Need for Reliable Resource Data: A 38 Year Database for Metocean and Wave Energy Assessments. Atmosphere 10 (9), 551. http://dx.doi.org/10.3390/atmos10090551, URL https://www.mdpi.com/2073-4433/10/9/551, Number: 9 Publisher: Multidisciplinary Digital Publishing Institute.

Levin, A., Glozman, M., Keren, Y., Trifonova, E., 2019. Processing of Hydrographic Data for the Haifa Region. Technical Report 893, CAMERI- Coastal and Marine Engineering Research Institute, Technion City, Haifa, p. 133.

López, M., Taveira-Pinto, F., Rosa-Santos, P., 2017. Influence of the power take-off characteristics on the performance of CECO wave energy converter. Energy 120, 686–697. http://dx.doi.org/10.1016/j.energy.2016.11.121, URL https://www.sciencedirect.com/science/article/pii/S0360544216317765.

Ma, K.-T., Luo, Y., Kwan, C.-T.T., Wu, Y., 2019. Mooring System Engineering for Offshore Structures. Gulf Professional Publishing.

Ma, S., Xu, D.-k., Duan, W.-y., Chen, J.-k., Liao, K.-p., Wang, H., 2020. The numerical study of viscous drag force influence on low-frequency surge motion of a semi-submersible in storm sea states. Ocean Eng. 213, 107511. http://dx.doi.org/10.1016/j.oceaneng.2020.107511, URL https://www.sciencedirect.com/science/article/pii/S0029801820305242.

Masoudi, E., Gan, L., 2021. Diffraction waves on general two-legged rectangular floating breakwaters. Ocean Eng. 235, 109420. http://dx.doi.org/10.1016/j.oceaneng.2021.109420, URL https://www.sciencedirect.com/science/article/pii/S0029801821008295.

Peña, E., Ferreras, J., Sanchez-Tembleque, F., 2011. Experimental study on wave transmission coefficient, mooring lines and module connector forces with different designs of floating breakwaters. Ocean Eng. 38 (10), 1150–1160. http://dx.doi.org/10.1016/j.oceaneng.2011.05.005, URL http://www.sciencedirect.com/science/article/pii/S0029801811000862.

Penalba, M., Touzón, I., Lopez-Mendia, J., Nava, V., 2017. A numerical study on the hydrodynamic impact of device slenderness and array size in wave energy farms in realistic wave climates. Ocean Eng. 142, 224–232. http://dx.doi.org/10.1016/j.oceaneng.2017.06.047, URL https://www.sciencedirect.com/science/article/pii/S0029801817303517.

Ray, J., 2000. WAMIT-MOSES Hydrodynamic Analysis Comparison Study. Technical Report, McDermott Engineering, LLC, JRME, URL http://bentley.ultramarine.com/hdesk/document/include/wamit_moses.pdf.

Sannasiraj, S.A., Sundar, V., Sundaravadivelu, R., 1998. Mooring forces and motion responses of pontoon-type floating breakwaters. Ocean Eng. 25 (1), 27–48. http://dx.doi.org/10.1016/S0029-8018(96)00044-3, URL https://www.sciencedirect.com/science/article/pii/S0029801896000443.

Solakivi, T., Kiiski, T., Kuusinen, T., Ojala, L., 2021. The European Ship Recycling Regulation and its market implications: Ship-recycling capacity and market potential. J. Clean. Prod. 294, 126235. http://dx.doi.org/10.1016/j.jclepro.2021.126235, URL https://www.sciencedirect.com/science/article/pii/S0959652621004558.

Subbulakshmi, A., Sundaravadivelu, R., 2021. Effects of damping plate position on heave and pitch responses of spar platform with single and double damping plates under regular waves. Ocean Eng. 224, 108719. http://dx.doi.org/10.1016/j.oceaneng.2021.108719, URL https://www.sciencedirect.com/science/article/pii/S0029801821001542.

Wan, Z., Wang, L., Chen, J., Sperling, D., 2021. Ship scrappage records reveal disturbing environmental injustice. Mar. Policy 130, 104542. http://dx.doi.org/10.1016/j.marpol.2021.104542, URL https://www.sciencedirect.com/science/article/pii/S0308597X21001536.

Wang, G., Drimer, N., Goldfeld, Y., 2020a. Modular floating structures (MFS) for offshore dwelling a hydrodynamic analysis in the frequency domain. Ocean Eng. 216, 107996. http://dx.doi.org/10.1016/j.oceaneng.2020.107996, URL http://www.sciencedirect.com/science/article/pii/S0029801820309458.

Wang, G., Goldfeld, Y., Drimer, N., 2019. Expanding coastal cities – Proof of feasibility for modular floating structures (MFS). J. Clean. Prod. http://dx.doi.org/10.1016/j.jclepro.2019.03.007, URL http://www.sciencedirect.com/science/article/pii/S0959652619306900.

Wang, G., Rosenfeld, Y., Drimer, N., Goldfeld, Y., 2020b. Occupant comfort analysis for rigid floating structures – methodology and design assessment for offshore dwelling module. Ships Offshore Struct. 1–16. http://dx.doi.org/10.1080/17445302.2020.1718267, URL https://www.tandfonline.com/doi/full/10.1080/17445302.2020.1718267.

Wehausen, J.V., Laitone, E.V., 1960. Surface Waves. In: Truesdell, C. (Ed.), Fluid Dynamics / StrÖmungsmechanik. In: Encyclopedia of Physics / Handbuch der Physik, Springer, Berlin, Heidelberg, pp. 446–778. http://dx.doi.org/10.1007/978-3-642-45944-3_6.

Yang, Y., 2016. Economic analysis on the 400K DWT VLOC (Ph.D. thesis). World Maritime University Dissertations. 1560.

Yang, Z., Xie, M., Gao, Z., Xu, T., Guo, W., Ji, X., Yuan, C., 2018. Experimental investigation on hydrodynamic effectiveness of a water ballast type floating breakwater. Ocean Eng. 167, 77–94. http://dx.doi.org/10.1016/j.oceaneng.2018.08.030, URL https://www.sciencedirect.com/science/article/pii/S0029801818315440.

Yeh, P.-H., Tsai, S.-Y., Chen, W.-R., Hsu, S.-M., Chen, B.-F., 2021. A platform for Kuroshio Energy Harvesters. Ocean Eng. 223, 108693. http://dx.doi.org/10.1016/j.oceaneng.2021.108693, URL https://www.sciencedirect.com/science/article/pii/S0029801821001281.

Zhao, W., Milne, I.A., Efthymiou, M., Wolgamot, H.A., Draper, S., Taylor, P.H., Eatock Taylor, R., 2018. Current practice and research directions in hydrodynamics for FLNG-side-by-side offloading. Ocean Eng. 158, 99–110. http://dx.doi.org/10.1016/j.oceaneng.2018.03.076.

Zhao, W., Wolgamot, H.A., Taylor, P.H., Taylor, R.E., 2017. Gap resonance and higher harmonics driven by focused transient wave groups. J. Fluid Mech. 812, 905–939. http://dx.doi.org/10.1017/jfm.2016.824, Publisher: Cambridge University Press.

Zhou, J., Ren, J., Bai, W., 2023. Survey on hydrodynamic analysis of ship–ship interaction during the past decade. Ocean Eng. 278, 114361. http://dx.doi.org/10.1016/j.oceaneng.2023.114361, URL https://www.sciencedirect.com/science/article/pii/S002980182300745X.